The 2015 World Congress on
Advances in Civil, Environmental, and Materials Research (ACEM15)
Incheon, Korea, August 25-29, 2015

Numerical Simulation of Bullet Impact for Rotorcraft Fuel Cell Assembly based on SPH

*Hyun-gi Kim[1)] and Sungchan Kim[2)]

[1), 2)] *Korea Aerospace Research Institute, 169-84 GwahangnoYuseong-gu, Daejeon, 305-806, Korea*
[1)] *shotgun1@kare.re.kr*

ABSTRACT

Military rotorcraft is constantly exposed to the risk of the bullet impacts because they operate in a battle environment. Since the bullet impact damage can be deadly to crews, the fuel cells of military rotorcraft must be designed by taking extreme situations into account. Fuel cell design factors to be considered include the internal fluid pressure, the structural stress, and the kinetic energy of the bullet. Verification testing using real objects is the best way to obtain these design data effectively, but, may be a big burden due to the huge cost and long-term preparation efforts. The use of various numerical simulations tests at an early design stage can reduce the risk of trial-and-error and improve prediction of performance. The present study investigated the effects of bullet impacts on fuel cells using numerical simulation based on SPH(smoothed particle hydrodynamic) conducted with the commercial package, LS-DYNA. Then, the resulting equivalent stress, the internal pressure and the kinetic energy of the bullet were evaluated in detail to examine the possible use of the numerical method to obtain configuration design data for the fuel cell

1. INTRODUCTION

The basic function of an aircraft fuel cell is to store fuel. However, a fuel cell has a significant influence on the survivability of crews in aircraft emergency situations. Thus, the fuel cell should be designed by considering predictable extreme situations, such as an internal explosion or fire, in order to improve the survivability of the crew. To prove the soundness of a fuel cell, the U.S. government has established a military specification, so called MIL-DTL-27422 (U.S. Army Aviation and Missile Command 2007), and requires the relevant test be performed under strict standards. In order to prove the soundness of a fuel cell, it is most preferred to carry out the verification test using the actual product. However, a verification test using the actual product requires considerable expense. In addition, the design and manufacturing of a fuel cell takes a long time. Moreover, the cost of manufacturing a fuel cell may be a burden. When the fuel cell test results in failure, the cost and time for further examination will affect the overall aircraft production period. For instance, the most well-known rotorcrafts

---

[1)] Senior Researcher
[2)] Principal Researcher

including the AH-64 Apache, UH-60 Blackhawk utility helicopter, and tilt rotor V-22 Osprey were all developed through several test failures and tough processes (Ugone *et al*. 2002).

For these reasons, performing various numerical analyses of the fuel cell prior to proof testing can minimize the reliance on trial and error, and its costs. Furthermore, important design information may be produced through the cooperative research, since these numerical analyses can accumulate test data for extended operating times. However, in the past there have been numerous limitations to conducting such complicated simulations, such as fluid-structure interactions (FSI), because they require significant amounts of computer resources. Recently, with advanced technological breakthroughs and developments in computing and specialized software, it has become more feasible to conduct research such as FSI using various scenarios.

This study carried out a numerical analysis of the FSI problem of the fuel cell assembly considering the situation in which a projectile hits a military rotary wing aircraft. There are two kinds of method for solving the FSI problem: the ALE method based on FEM, and the element free method, such as smoothed particle hydrodynamics (SPH).

ALE sets up a Lagrangian mesh for the structure and Eulerian mesh for the fluid. This method can provide accurate results because it interchanges the interface information between the structure and fluid. However, it requires excessive computing time and computer resources. Moreover, under high-level impact conditions, ALE is liable to fail in a contact situation due to excessive deformation of meshes. Furthermore, it can cause fluid to leak out of the interface. SPH is based on the Lagrangian methodology. SPH assumes that each particle represents a material property within in a specific domain. Even though SPH requires a large number of particles for detailed fluid simulations, it can solve the FSI problem quickly compared to the ALE method. Regardless of twisted or excessive deformations, fluid does not leak out of the interface so long as the contact conditions are well set up between both interfaces. After considering the efficiency of the computing cost and propriety of the numerical simulations, this study employed the SPH method for the FSI analysis. The focus of this study was an FSI simulation based on SPH involving a bullet impact of a rotorcraft fuel cell assembly using the commercial package LS-DYNA.

When a fuel cell is penetrated by anti-aircraft fire, there may be an internal explosion due to the sudden rise of internal fluid pressure. Moreover, once the bullet is inside the fluid, since the bullet's movement changes irregularly, it is possible that it may have a fatal effect on the health of the fuel cell itself and internal attachments. Empirically, the bullet is likely to puncture the exit portion in the inclined posture. When the bullet hits with high kinetic energy, it may also endanger the survival of the aircraft and crew by causing excessive fuel leakage. In view of these emergency situations, in this present study, critical design information such as the behavior of the bullet, the internal fluid pressure and the stress values have been estimated. Furthermore, by evaluating how changes in the kinetic energy of the bullet affect the fuel cell, we approached the possibility of acquiring design data to help prepare for a bullet impact situation.

This study considers the real time dynamic behavior of the fuel cell assembly and the internal fluid under a bullet impact load using an explicit method. The equivalent stress was calculated for each fuel cell and the weak area of the fuel cell assembly was

investigated under a bullet impact load.

The remainder of this paper is organized as follows. Section 2 briefly introduces the methodology of the SPH. Section 3 explains the conditions for the numerical simulation including the material information and analysis model using FEM and SPH. Finally, Section 4 presents the results of the numerical simulations of the bullet impact.

2. Review of Smoothed Particle Hydrodynamics

SPH represents large deformations well because it does not have fixed connectivity between particles. This method can be easily applied to complex geometries and large-scale features are easy to obtain by tracing the particle motion. Because of these advantages, SPH has been primarily applied to shock simulations, free surface flows, and sound propagation (Monaghan *et al*.1983, Monaghan 1992, Herreros *et al*. 2011, Shao *et al*. 2012, Marongiu *et al*. 2010). Recently, it has been effectively applied to high explosive simulations and high velocity impact computation (Liu *et al*. 2003, Liu *et al*. 2013, Johnson *et al*. 1996).

The field values of each particle, $\langle f(x)\rangle$ are evaluated using the smoothing kernel function. The SPH formation is presented in Eq. (1), as follows:

$$\langle f(x)\rangle = \int_{\Omega} f\left(x^{'}\right) W\left(x-x^{'},h\right) dx^{'} = \sum_{j=1}^{N} \frac{m_j}{\rho_j} f\left(x_j\right) W\left(x-x_j,h\right) \tag{1}$$

Here, $W(x)$ is the smoothing kernel function, ρ is the particle density, m is the particle mass, *h* is the smoothing length, and $f\left(x_j\right)$ is the physical value at the *j* position.

The cubic spline function is mainly used for the smoothing kernel function as given in Eq. (2).The smoothing kernel function, $W(x)$ should satisfy the three kinds of condition presented in Eq. (3) to Eq. (5).

$$W\left(r,h\right) = \frac{8}{\pi h^3} \begin{cases} 1-6\left(\frac{r}{h}\right)^2 + 6\left(\frac{r}{h}\right)^3 & 0 \le \frac{r}{h} \le \frac{1}{2} \\ 2\left(1-\frac{r}{h}\right)^3 & \frac{1}{2} \le \frac{r}{h} < 1 \\ 0 & \frac{r}{h} \ge 1 \end{cases} \tag{2}$$

Normalization condition : $\int_{\Omega} W\left(x-x^{'},h\right) dx^{'} = 1$ (3)

Delta function property : $\lim_{h\to 0} W\left(x-x^{'},h\right) = \delta\left(x-x^{'}\right)$ (4)

Compact condition : $W\left(x-x^{'},h\right) = 0$ when $\left|x-x^{'}\right| > \kappa h$ (5)

In Eq. (5), *κ* is a constant value that defines the effective non-zero area in the smoothing kernel function.

In SPH, the continuity equation, momentum equation, and energy conservation are discretized as described in Eqs. (6) to (8). These equations are evaluated at each time step by the explicit integration procedure (Hahn 2009, Naval Surface Weapons Center 1997).

$$\text{Continuity equation: } \frac{d\rho_i}{dt} = \sum_j m_j \left(v_i - v_j\right) \nabla_i W_{ij} \tag{6}$$

$$\text{Momentum equation : } \frac{dv_i}{dt} = -\sum_j m_j \left(\frac{p_j}{\rho_i^2} + \frac{p_i}{\rho_j^2} \right) \nabla_i W_{ij} \tag{7}$$

$$\text{Energy conservation : } \frac{du_i}{dt} = \frac{1}{2} \sum_j m_j \left(\frac{p_j}{\rho_i^2} + \frac{p_i}{\rho_j^2} \right) v_{ij} \nabla_i W_{ij} \tag{8}$$

Here, ∇_i is a Laplacian operator.

However, SPH has a defect in shock problem and, therefore, it uses an artificial viscosity in order to improve its shock capturing abilities. The artificial viscosity functions as a resistive pressure and thermalizes the kinetic energy in the shock while converting it into thermal energy. Then, this artificial viscosity term is added to the momentum and energy equations as follows.

$$\text{Momentum with artificial viscosity : } \frac{dv_i}{dt} = -\sum_j m_j \left(\frac{p_j}{\rho_i^2} + \frac{p_i}{\rho_j^2} + \Pi_{ij} \right) \nabla_i W_{ij} \tag{9}$$

$$\text{Energy with artificial viscosity : } \frac{du_i}{dt} = \frac{1}{2} \sum_j m_j \left(\frac{p_j}{\rho_i^2} + \frac{p_i}{\rho_j^2} + \Pi_{ij} \right) v_{ij} \nabla_i W_{ij} \tag{10}$$

where, artificial viscosity $\Pi_{ij} = \begin{cases} \dfrac{-\alpha \hat{c}_{ij} \mu_{ij} + \beta \mu_{ij}^2}{\rho_{ij}} & v_{ij} \cdot \gamma_{ij} < 0 \\ 0 & v_{ij} \cdot \gamma_{ij} > 0 \end{cases}$

$\hat{c}_{ij}$ is the mean sound speed at position i and j. $\mu_{ij} = \dfrac{h v_{ij} \cdot \gamma_{ij}}{\gamma_{ij}^2 + \eta^2}$

3. Conditions for Numerical Analysis

3.1 Material Information and Configuration of Fuel Cell Assembly

As seen in Fig.1, the fuel cell material largely consists of three layers. The reinforcing layer supports the external load. In detail, the nylon 66 molded into the rubber decides the stiffness value of the reinforcing layer. The self-sealing material layer is placed between the reinforcing layers. It repairs the damaged area by swelling of its sponge structure after being punctured.

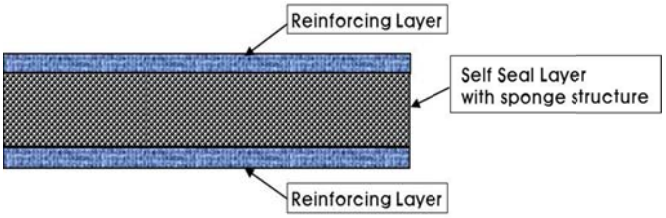

Fig. 1 Section of fuel cell material

The overall configurations of fuel cell assembly are presented in Fig. 2 and 3. The names of each fuel cell component and other critical components such as metal fittings are given in the figures. The fuel cell assembly consists of two groups: the left group and the right group. The left group has the after fuel cell (AFT) and second feeder fuel cell (FC2). The right group has the forward fuel cell (FWD) and first feeder fuel cell (FC1). The FWD and AFT stores fuel; the FC1 and FC2 transfer the fuel into the engine through the booster pump. Thus, the FC1 and FC2 are called feeder cells.

The numerical model consists of a bulkhead, fuel cell assembly, and plumbing. Each fuel cell consists of a metal fitting and skin. Mooney-Rivlin material model is employed for fuel cell skin and the material data has been acquired from the previous research (Kim *et al*. 2014). The metal fitting is mainly used to install the line replacement unit (LRU) or attach the fuel cell on the fuselage. As provided in Table 1, the material of the bulkhead, metal fitting, and plumbing is aluminum. The thicknesses of the bulkhead and plumbing are 2.0mm; the metal fitting is 10.0mm and the skin is 10.0mm.The diameter of the bullet is 14.5mm and its material type is assumed to be a rigid body with cylindrical configuration. The velocity of the normal bullet is 900m/s~1,000m/s. This study sets the initial bullet speed to 650m/s by assuming the conditions of striking a rotorcraft from 800m away.

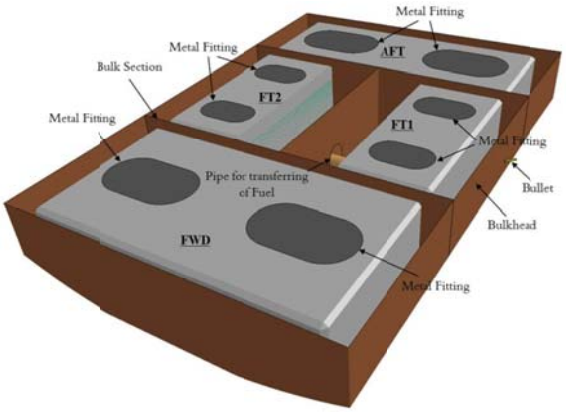

Fig. 2 Numerical Simulation Model of Fuel Cell Assembly

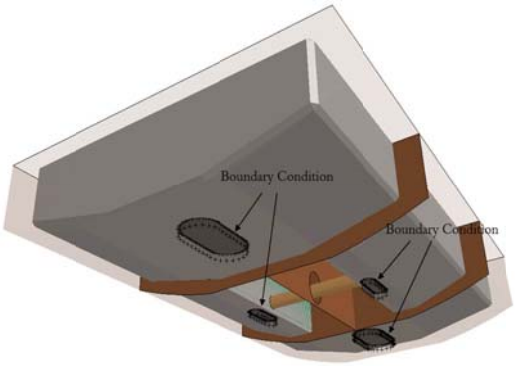

Fig. 3 Boundary Condition imposed on Bottom

Table 1 Input Data of Materials for the Numerical Simulation

Part	Input Data
Fluid	▪ Density : 998kg/m3
Skin of fuel cell	▪ Material model : Mooney-Rivlin Material ▪ Density : 980kg/m3 ▪ Poisson ratio : 0.49 ▪ Thickness : 10mm
Metal fitting, Bulkhead Plumbing	▪ Material model: Piecewise linear plasticity ▪ Density : 2,867kg/m3 ▪ Young's modulus : 72.4GPa ▪ Poisson ratio : 0.33 ▪ Thickness $\begin{cases} metal\ \ fitting : 10mm \\ bulkhead,\ plumbing : 2mm \end{cases}$
Bullet	▪ Material model : Rigid ▪ Density : 17,000 kg/m3 ▪ Young's modulus : 370GPa ▪ Poisson ratio : 0.17 ▪ Diameter : 14.5mm ▪ Initial speed : 650 m/s

3.2 Finite Element Model for Numerical Simulation

The finite element model is constructed as displayed in Fig.4. The total number of shell elements for the fuel cell assembly is 68,641. In detail, the FWD is constructed with 21,200 shell elements and the AFT has 15,541 shell elements, FT1 has 10,005 shell elements and FT2 has 10,003 shell elements. The bulkhead is constructed with 16,165 shell elements. The internal fluid is filled with 1,207,614 particles. To ensure the results of the FSI analysis, the contact condition between the structure and fluid should be well defined. This study applies the contact keywords provided in LS-DYNA, e.g. single surface, node-to-surface, and surface-to-surface. All contact conditions between each part are given in Table 2.

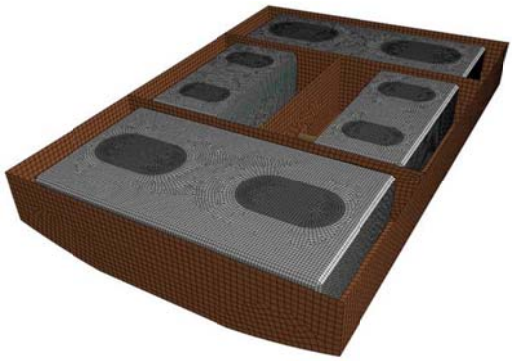

Fig. 4 Finite Element Model(section from top view)

Table 2 Contact conditions for numerical simulation of crash impact

Contact condition	Applied Part
Single Surface	▪ fuel cell group ▪ bulkhead
Node to Surface	▪ fuel cell group ↔ fluid particle ▪ plumbing ↔ fluid particle ▪ bulkhead ↔ fluid particle ▪ bullet ↔ fluid particle
Surface to Surface	▪ bulkhead ↔ fuel cell group ▪ bulkhead ↔ bullet

4. Result of Numerical Simulation

4.1 Impact on the Single Fuel Cell

Before simulating the bullet impact for the entire fuel cell assembly, simulation of a single fuel cell was performed, to obtain validation of the numerical model.

Fig.5 shows the numerical model for the single fuel cell and the boundary condition imposed on the metal fitting on the bottom, and Fig.6 presents the structure and fluid section. A four nodes shell element is applied for the structural section, and the internal fluid with 85% volume is modeled by particles. The total number of shell elements and particles is 41,598 and 408,771, respectively.

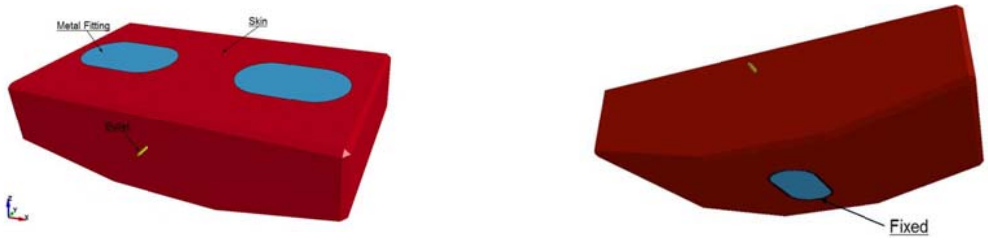

a) Configuration of Fuel Cell for Numerical Analysis

(b) Boundary Condition

Fig. 5 Configuration of Fuel Cell and Boundary Condition for Numerical Analysis

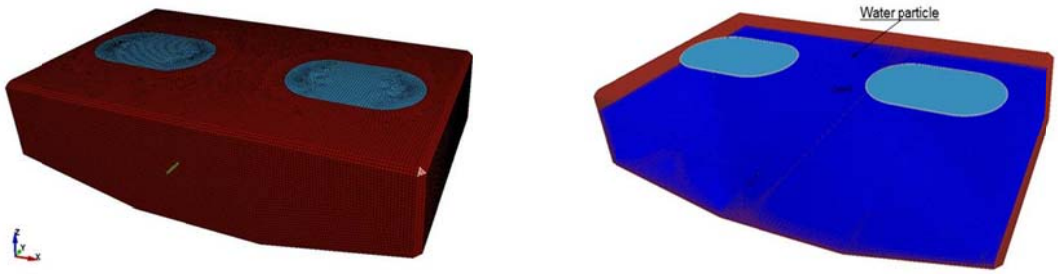

(a) FEM for Structure

(b) Particle for Internal Fluid

Fig. 6 Numerical Model for Structure and Internal Fluid

The first numerical example reflects the case where a 14.5mm diameter bullet directly impacts at a speed of 650m/s. Numerical analysis was performed in between 0.00~0.01 seconds with a 1.3×10^{-7} time step. Fig. 7 shows the effect on the internal fluid and the behavior of the bullet through the fuel cell from the moment of striking the outer skin. Because the bullet lost energy and overturned due to fluid resistance, a relatively larger area than the incident portion is damaged upon impact when the bullet exits.

A hydraulic ram effect is produced by the rapid increase of internal pressure. It acts as a shock load on the skin and metal fittings. Considering this, the result of the equivalent stress distribution is shown in Fig. 8. The maximum equivalent stress of the metal fitting and skin is calculated to be 260MPa(@5.4ms) and 121MPa(@4.6ms), respectively. Fig. 9 shows the deformed configuration of the exit portion. Compared to the damage of the incident portion, the damage to the exit part is large due to the bullet overturning.

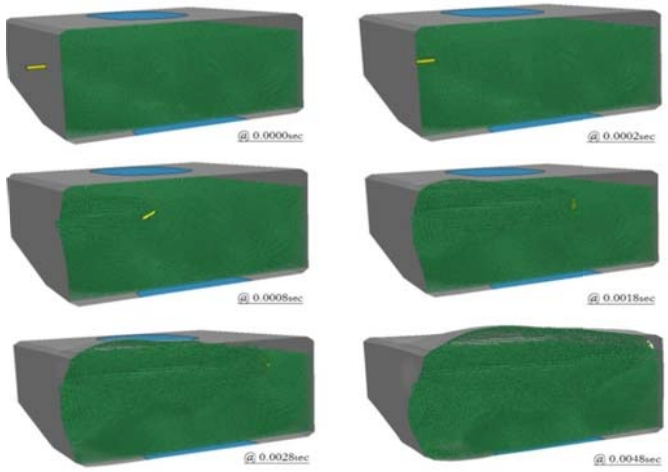

Fig. 7 Behavior of the Bullet in the Internal Fluid over Time

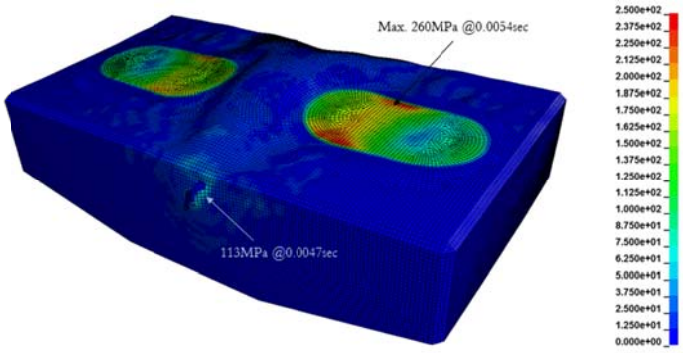

Fig. 8 Maximum Equivalent Stress at Critical Time

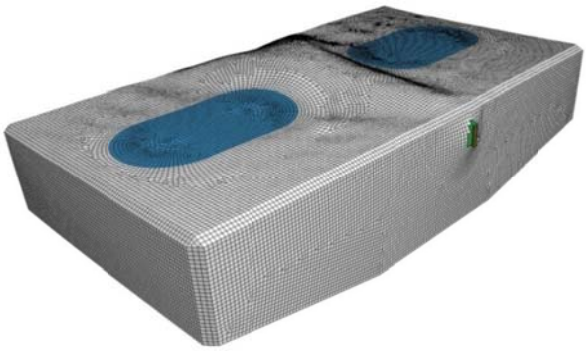

Fig. 9 Emitting Moment of Bullet at Exit Portion

Fig. 10 is the distribution of the internal pressure of the fluid particles from entry to exit. As shown in Fig.10, at the moment of impact to the incident portion(@0.2ms), the maximum pressure is calculated to be 368MPa. After this moment, the kinetic energy of the bullet is reduced, and the internal pressure also decreases to less than 200MPa. The kinetic energy of the bullet at the exit section is calculated to be 595J. A bullet with a kinetic energy of this level is considered to have penetrated the outer skin by causing a greater stress than the failure criteria of the fuel cell material. From entry to exit, the change in kinetic energy of the bullet is given in Fig.11.

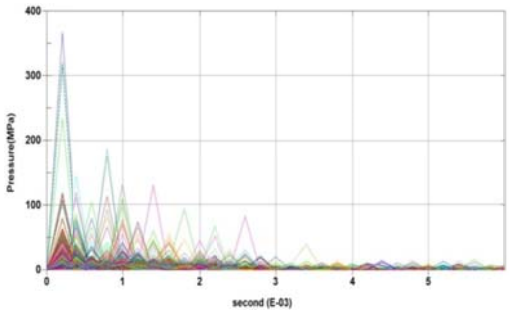

Fig. 10 Change of the internal pressure

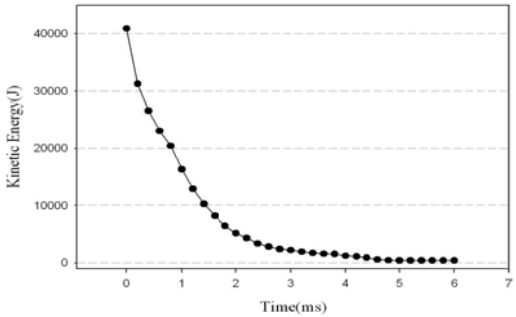

Fig. 11 Change in kinetic energy of the bullet

Fig.12 shows the behavior of the internal fluid and bullet if the bullet is shot from an oblique angle with the same bullet and speed conditions. At the moment of bullet impact on the entry section, the internal pressure rapidly increases to 357MPa, as shown in Fig.13. After that, due to the resistance of the inner fluid, the internal pressure

is reduced to less than 200MPa.

Similar to the result shown in Fig.7, in the process of going through the internal fluid, the bullet is overturned. This behavior produces the hydraulic ram and results in the bending force on the metal fittings. As shown in Fig.14, the maximum equivalent stress on the metal fitting is calculated to be 342MPa. After hitting the exit portion, the speed of the bullet is reduced to 52.6m/s and the kinetic energy is calculated to be 301J at that moment. By impacting in a diagonal direction the bullet does not penetrate the exit portion, because its kinetic energy has been reduced after going through a longer distance of fluid, as compared to the straight impact case.

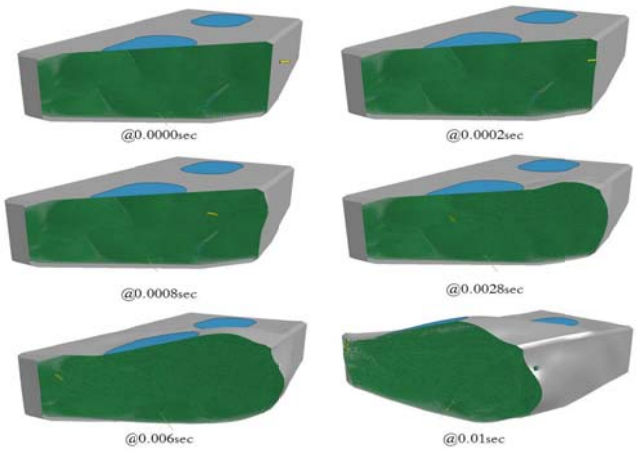

Fig. 12 Behavior of the Bullet in the Internal Fluid over Time

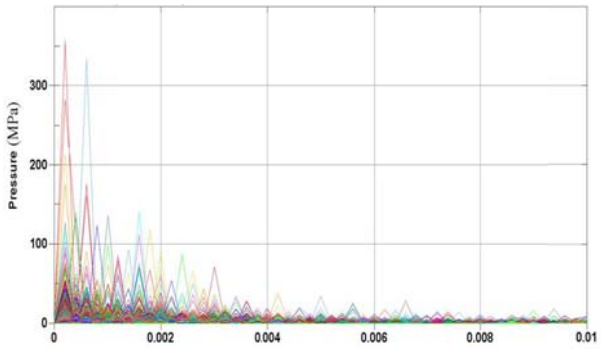

Fig. 13 Change of the internal pressure

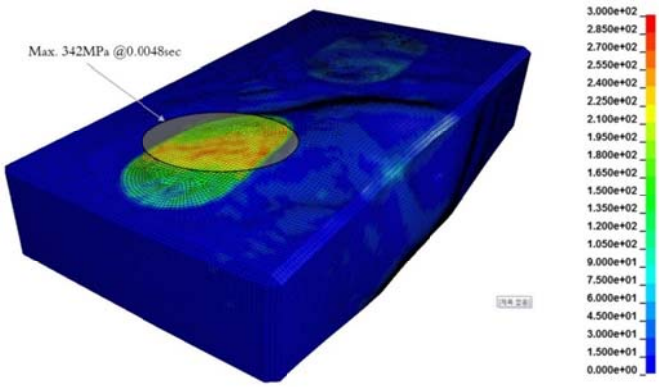

Fig. 14 Maximum Equivalent Stress on the Metal Fitting

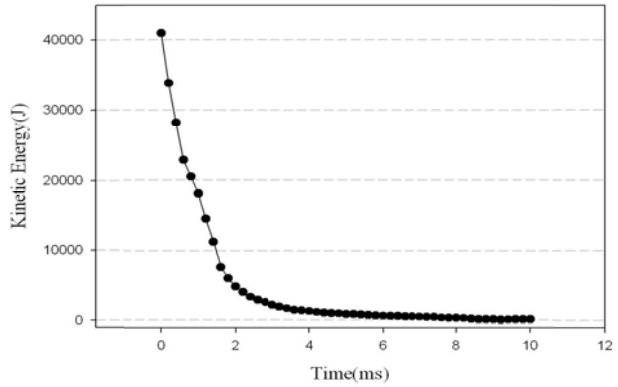

Fig. 15 Change of Kinetic Energy over Time

4.2 Impact on the Full-scale Fuel Cell Assembly

Numerical simulations were performed for side impacts of the FT1 and FWD from a relative angle of 45deg. under the same impact conditions. Analysis time was 0~0.015 seconds and the time step was 1.97×10^{-7} second. It took about 48 hours with 64 bit computers.

4.2.1 Impact on the side of Feeder Cell

<u>Internal Behavior, Pressure and Energy</u>

Fig. 16 shows the behavior of the internal fluid after the bullet impact on the left side of the FT1. After being discharged toward the side of the FT1 at a 45deg. angle, the bullet penetrates the bulkhead, FT1 and FWD progressively. In this process, significant damage is produced at the entry area of the FWD by the overturning bullet.

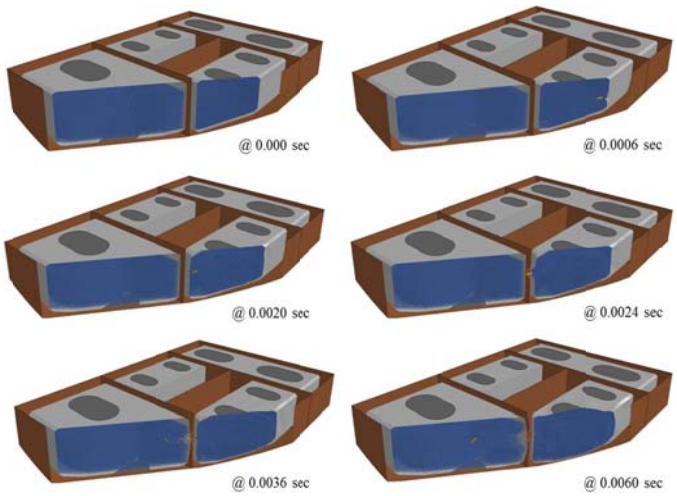

Fig. 16 Behavior of Internal Fluid &Bullet(Section View)

Fig. 17 and 18 show the results of the internal pressure of FT1 and FWD over time. Maximum pressure is calculated to be 295MPa and 98MPa in FT1 and FWD, respectively. Since the projectile flight lasts for a very short time, the internal pressure tends to decrease dramatically after 2ms. As shown in Fig.17, the internal pressure of FT 1 jumps at 0.6ms, then, is reduced more than 70% after 2.0ms due to the sudden loss of kinetic energy. Since that bullet goes through the bulkhead and FT1, it was calculated to produce a relatively low internal pressure in the FWD because of its great amount of energy loss.

Fig. 19 shows the change in kinetic energy of the bullet over time. At the initial impact moment, its kinetic energy is calculated to be 38,300J. Then, when the bullet impacts the FWD after penetrating the FT1 and bulkhead, its kinetic energy has been reduced to 85%, which is calculated to be about 6,070J. Then, the kinetic energy of the projectile is reduced to 380J(@10.2ms) after going internally through the FWD. It has been estimated that with a kinetic energy of this level the bullet cannot pass through the fuel cell.

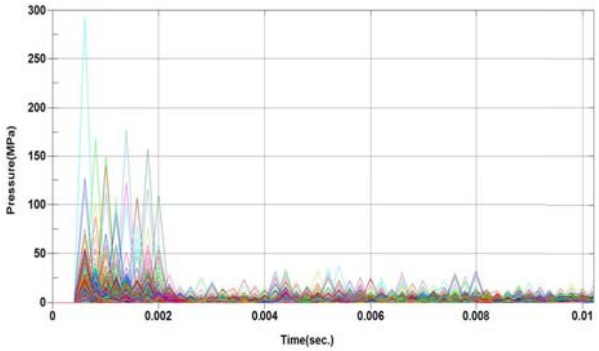

Fig. 17 Internal Pressure in FT1(Max.@0.6ms)

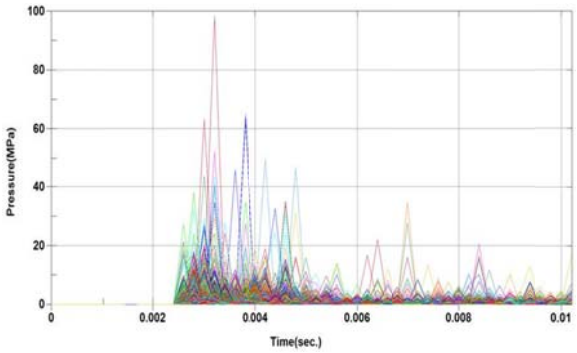

Fig. 18 Internal Pressure in FWD(Max.@3.2ms)

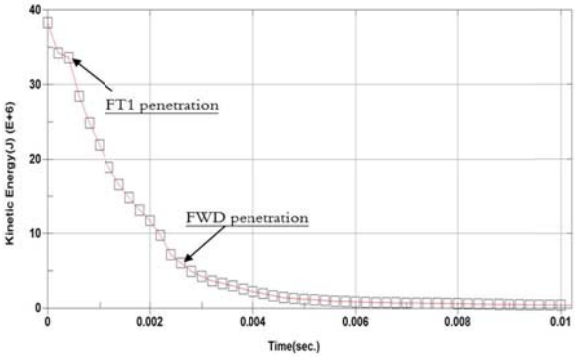

Fig. 19 Kinetic Energy of Bullet

Estimation of Equivalent Stress

Fig. 20 is the deformed configuration of the fuel cell at the time when the maximum equivalent stress occurs. The maximum equivalent stress, 321MPa, is produced on the upper metal fitting of FT1. Maximum equivalent stress is generated at the time that the bullet reaches the FWD through FT1. This is the reason why the hydraulic ram affects the fuel cell with a time difference. The internal behavior of the fluid at that moment is shown in Fig.21. While the bullet initially penetrates the fuel cell, the internal fluid is pushed forward suddenly. As this behavior results in a bending effect, the maximum stress occurs on the upper metal fitting. The material of the metal fitting is Aluminum 2014 T6. Considering a tension strength of 485MPa (yield strength 415MPa), it is estimated that the metal fitting has a safety factor of 1.3 times. Fig. 22 shows the distribution of the equivalent stress on the fuel cell skin with the exception of the area directly damaged by the bullet. Similar to Fig.8, because of the time difference of the hydraulic ram, the maximum stress value, 73MPa, is shown in the area around the metal fittings after the bullet has already been through (@9.8ms). Due to the bending load, tensile load acts on the skin of the fuel cell. From the results of a specimen test, the damage strength of the skin material was measured to be 144.89MPa. Then, it can be estimated that the skin area of the fuel cell has more than twice safety factor.

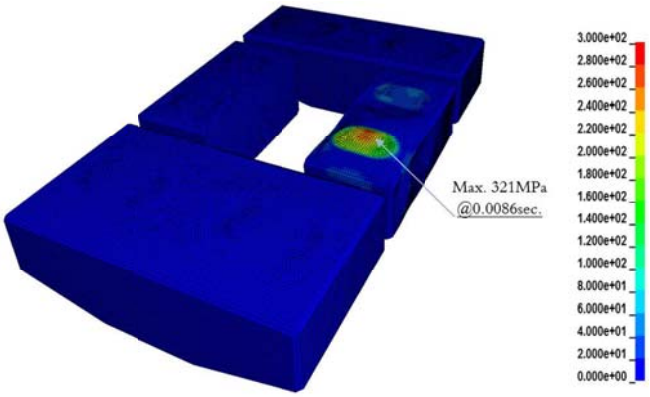

Fig. 20 Maximum Equivalent Stress at Critical Time(@8.6ms)

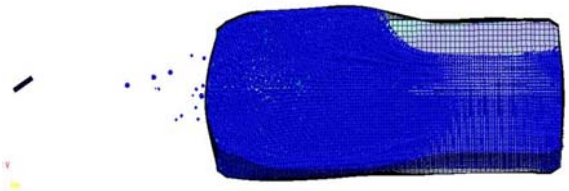

Fig. 21 Behavior of Internal Fluid at the Critical Time(@8.6ms)

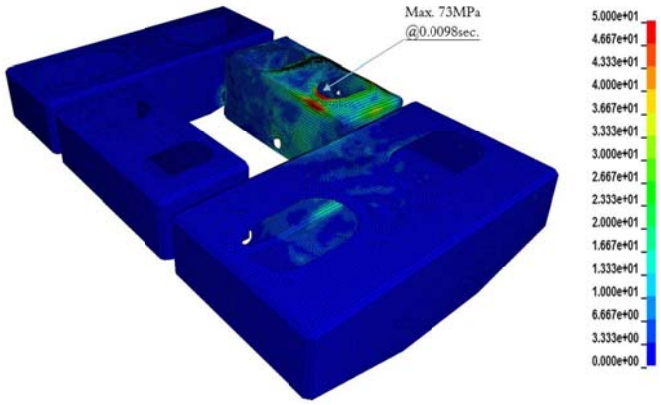

Fig. 22 Maximum Equivalent Stress on the Skin except the Damaged Area

4.2.2 Impact on the side of FWD

Fig. 23 presents the behavior of the internal fluid when the bullet impacts the FWD from the 45 deg. angle direction. When the FWD is penetrated at 0.6ms, the kinetic energy of the bullet is calculated to be 28,500J. After that, the bullet successively penetrates the backward wall of the FWD and the forward wall of the FT1 and the change of kinetic energy is shown in Fig. 24. Compared to the initial kinetic energy, the kinetic energy of the bullet is then calculated to be 1,030J, a decrease of more than 90% in the process of penetrating FT1. In this process, the bullet is tumbled and a large amount of damage occurs in the exit section, as shown in Fig.25. After penetrating the FT1, the bullet impacts the exit area at 4.2ms. At this time the kinetic energy of the bullet is calculated to be 501J. It is concluded that a bullet with kinetic energy of this

level does not penetrate the fuel cell material. Fig.26 shows the pressure distribution of the internal fluid in the FWD. Maximum pressure is calculated to be 325MPa(@0.6ms). After 1ms, the kinetic energy and the internal pressure are reduced to less than 100MPa. As shown in Fig.27, the impact load caused by the hydraulic ram influences the metal fittings as a bending load. As a result, the maximum equivalent stress on the metal fittings is calculated to be 238MPa, which is considered to be a low value compared to hitting the side of FT1. The reason the hydraulic ram is more concentrated on the fuel cell is because of the narrow space and short distance between edges. This can be shown by comparing Fig. 21 and 27. Based on this, the equivalent stress of FT1 is determined to be higher than that of FWD.

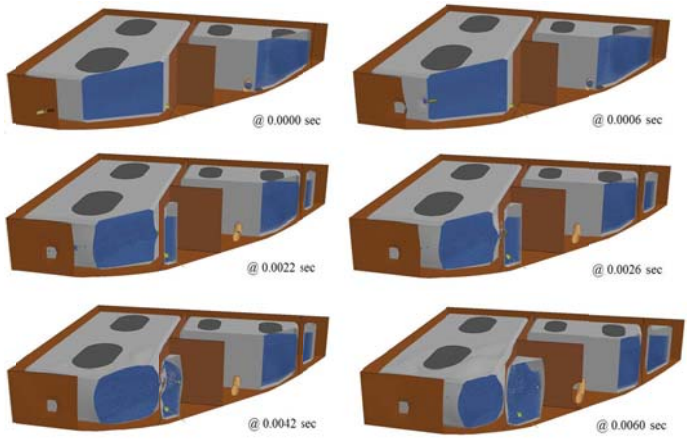

Fig. 23 Behavior of Internal Fluid &Bullet(Section View)

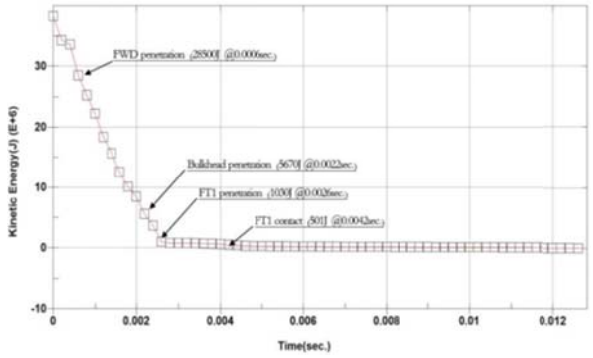

Fig. 24 Kinetic Energy of Bullet

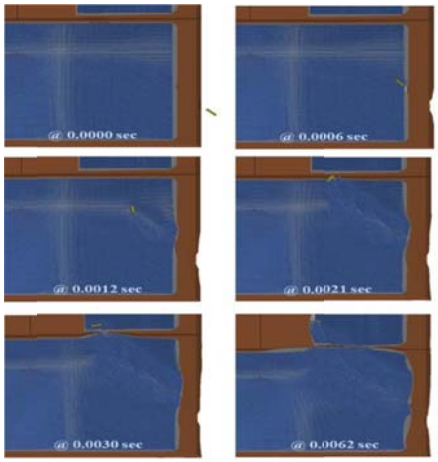

Fig. 25 Behavior of Tumbled Bullet(Top view)

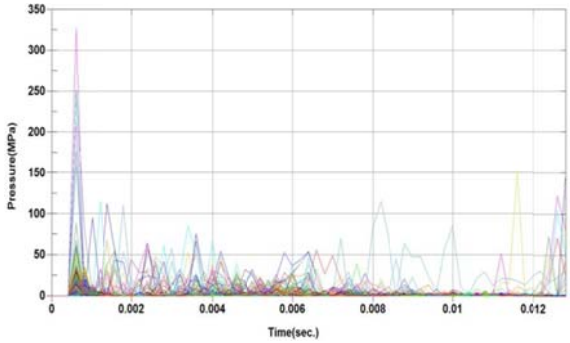

Fig. 26 Internal Pressure in FWD(Max.@0.6*ms*)

Fig. 27 Behavior of Internal Fluid at the Critical Time(Max. of Equivalent Stress)

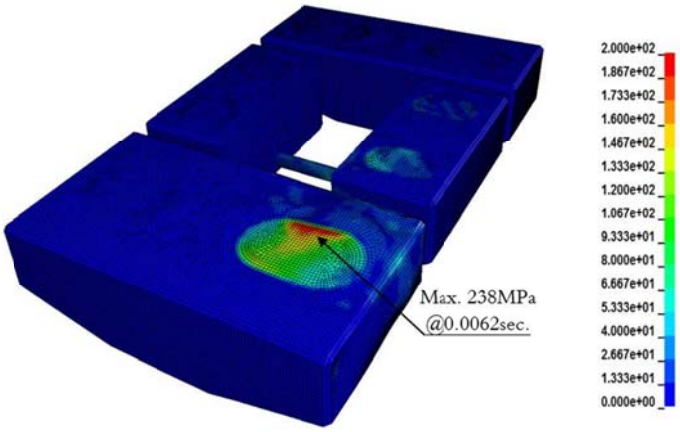

Fig. 28 Maximum Equivalent Stress at the Critical Time(@6.2*ms*)

5. CONCLUSIONS

This study presented an FSI analysis based on SPH simulating bullet impacts with a full-scale fuel cell assembly. The validity of the commercial software (LS-DYNA) for the application was demonstrated through numerical example. The behavior of the bullet was investigated by numerical results and the fluid pressure caused by the bullet impact and trajectory was calculated. Moreover, the maximum stress value was calculated and based on that data, vulnerable areas were estimated in each fuel cell.

Numerical analysis was performed for two cases, where the bullet impacted the fuel assembly perpendicular to its side, and from a 45 deg. angle. In both cases, the portion of the fuel cell where the bullet exited was severely damaged because the bullet was overturned in the process of penetrating the internal fluid. In the simulation result, it was estimated that the bullet could not penetrate the internal fuel cell skin to exit if its kinetic energy was reduced under 500J.Due to the creation of a hydraulic ram, the maximum stress primarily occurred on the top metal fittings. In detail, the maximum equivalent stress was calculated to be 321MPa in a side impact of the FT1 and 238MPa for the FWD. The maximum equivalent stress of the skin occurred around the top metal fitting of the FWD and its value was calculated to be 73MPa.Considering the results of the specimen test, it was estimated that the fuel cell skin was not damaged as a result of the bullet impact because it was capable of surviving twice that impact, i.e., that was its safety factor.

This study only performed numerical simulations considering a bullet impact to the side of the FWD and FT1 in the fuel cell assembly, and considering only bulkhead and fuel cells. However, there could be a much more severe case involving a bullet impact in the fuel cell assembly. Therefore, to improve the crew's survivability, various additional critical conditions need to be considered in the design of the fuel cell assembly. This study shows that there are various design parameters which can affect the bullet resistance capability of fuel cells. In the future, the reliability of the numerical simulations acquired in this study should be verified and, if necessary, the data correlation approach between the numerical simulation and actual test should be conducted. Moreover, this study will be extended to include estimations of bullet impact to a full-scale airframe coupled with an internal LRU and surrounding components.

REFERRENCES

Hahn, Philipp (2009), “On the use of meshless methods in acoustic simulations”, Thesis of Master, University of Wisconsin, Madison, WI

Herreros, M.I., Mabssout, M. (2011), “A two-steps time discretization scheme using the SPH method for shock wave propagation”, *Comput. Methods Appl. Mech. Engrg*., **200**, 1833–1845.

Jean-Christophe Marongiu, Francis Leboeuf, JoËlle Caro, Etienne Parkinson (2010), “Free surface flows simulations in pelton turbines using a hybrid SPH-ALE method”, *J. Hydraul. Res.*,**48**(1), 40-49

Johnson, G., Stryk, R., Beissel, S. (1996), “SPH for high velocity impact computations”, *Comput. Methods Appl. Mech. Engrg*., **139**, 347-373

Kim, Hyun-Gi, Kim, Sung Chan (2014), “Numerical simulation of crash impact test for fuel cell group of rotorcraft”, *Int. J. Crashworthines*.,**19**(6), 639-652

Liu, M., Liu, G., Zong, Z., Lam, K. (2003), “Computer simulation of high explosive explosion using smoothed particle hydrodynamics methodology”, *Comput. Fluids*, **32**(3), 305-322

Liu, M., Feng, D.L., Guo, Z.M. (2013), “Recent developments of SPH in modeling explosion and impact problems”, *International Conference on Particle-based Methods-Fundamentals and Applications*, Stuttgart, Germany, September

Monaghan, J., Gingold, R. (1983), “Shock simulation by the particle method SPH”, *J. Comput. Phys*., **52**(2), 374-389

Monaghan, J. (1992), “Smoothed particle hydrodynamics”, *Annu.Rev. Astron.Astr*., **30**, 543-574

Naval Surface Weapons Center (1997), “Prediction of Impact Pressures, Forces, and Moments during Vertical and Oblique Water Enter”, NSWC/WOL/TR77-16

Shao, J.R., Li, H.Q, Liu, G.R., Liu, M.B. (2012), “An improved sph method for modeling liquid sloshing dynamics”, *Comput. Struct*., **100-101**, 18-26

Ugone, Mary L., Meling, John E., Snider, Jack D., Gause, Neal J., Carey, Alice F. (2002), “Acquisition: Fuel Cells of the V-22 Osprey Joint Advanced Vertical Aircraft”, D-2003-013

U.S. Army Aviation and Missile Command (2007), “Detail Specification for the Tank, Fuel, Crash-Resistant, Ballistic-Tolerant, Aircraft”, MIL-DTL-27422D